Generic spatiotemporal dynamics near codimension-two Turing-Hopf bifurcations

M. Meixner,[1] A. De Wit,[2] S. Bose,[1] and E. Schöll[1]
[1]*Institut für Theoretische Physik, Technische Universität Berlin, Hardenbergstraβe 36, D-10623 Berlin, Germany*
[2]*Service de Chimie Physique and Centre for Nonlinear Phenomena and Complex Systems and Nonlinear Chemistry Unit, Case Postale 231, Université Libre de Bruxelles, Campus Plaine, B-1050 Brussels, Belgium*
(Received 9 December 1996)

The coupling of spatial and temporal symmetry breaking instabilities is studied in a two-variable reaction-diffusion model describing semiconductor transport. A variety of spatiotemporal patterns corresponding to pure Hopf and Turing modes, localized patterns, and mixed Turing-Hopf modes including subharmonic spatiotemporal spiking are found. By organizing the results in a time-scale versus space-scale diagram, and by comparing them with a chemical reaction-diffusion model, it is shown that such behavior is generic for a class of extended nonlinear dynamic systems near codimension-two Turing-Hopf bifurcations.
[S1063-651X(97)09906-6]

PACS number(s): 05.45.+b, 72.20.Ht

I. INTRODUCTION

Studies of dynamics resulting from the coupling between two different instabilities have recently received renewed attention as new experimental results have become available. In particular, focus has been put on the coupling between instabilities breaking spatial and temporal symmetries, respectively. The interaction of an instability leading to steady spatial structures with a Hopf instability giving rise to temporal oscillations indeed yields interesting spatiotemporal dynamics, as observed experimentally in fields as diverse as hydrodynamics [1,2], resistively coupled electronic oscillator networks [3] or chemical systems [4,5]. Such dynamics are obtained for values of parameters allowing for degeneracy between the thresholds of the two instabilities, i.e., near a codimension-two point. Several analyses have already classified the different bifurcation scenarios occurring near a codimension-two steady Hopf point [6–10]. The predicted types of dynamics range from steady Hopf bistability and localized structures to stationary states mixing spatial organization and Hopf-type oscillations. Several of these have been recovered in a chemical reaction-diffusion model [10] featuring interaction between a Hopf instability and a Turing instability [11] which gives rise to a steady spatial patterning of the concentrations. Some of these behaviors are relevant to experimental observations in the chlorite-iodide-malonic acid reaction [4,5] featuring a codimension-two Turing-Hopf point (CTHP). The Turing mechanism of spatial pattern formation relies on the coupling between nonlinear kinetics and molecular diffusion. Such a diffusion-driven instability can be recovered in other fields like electron-hole plasmas in semiconductors, gas discharge devices, heterogenenous catalysis, or semiconductor devices, for example [12]. The aim of this paper is to show that the spatiotemporal dynamics predicted near a CTHP can be recovered in a semiconductor model. A comparison of this semiconductor model and of a chemical reaction-diffusion model shows that a generic classification of the spatiotemporal dynamics is possible near the codimension-two Turing-Hopf point.

In semiconductor charge transport, the bifurcation of spatiotemporal patterns has been extensively studied in recent years [13–16]. While many models yield Hopf bifurcations of spatially homogeneous limit cycles [17], Turing instabilities are less common in semiconductor transport [15,18]. The properties of localized structures have been studied theoretically in detail by several groups [24–29] in reaction-diffusion systems. Another elementary spatiotemporal pattern, which has been observed experimentally in various different semiconductor devices, e.g., layered structures like p-n-p-n diodes [19,20] and p-i-n diodes [21], or in impurity impact ionization breakdown [22,23], is the *spatiotemporal spiking mode*. A simple, generic model [30] which displays such spiking behavior, as well as transient spatiotemporal chaos [31], independently of the specific microscopic transport mechanism that is effective in a particular semiconductor device [32], has been proposed. It is a two-component reaction-diffusion system of activator-inhibitor type. Such activator-inhibitor systems are widely used in the description of active media, not only in semiconductor transport but also in chemical reaction systems [33,34]. In this paper we present a detailed investigation of this reaction-diffusion model, and show that one of its characteristic features is the possibility of a codimension-two Turing-Hopf bifurcation. We find a rich variety of spatiotemporal patterns near the codimension-two Turing-Hopf point, of which the spiking mode is only one example. Our findings support the view that such spatiotemporal dynamics is generic for the coupling of spatial and temporal instabilities in a large class of extended nonlinear systems.

The paper is organized as follows. In Sec. II, we present our semiconductor model and study its linear stability. In Sec. III, the different types of spatiotemporal dynamics predicted in the vicinity of a codimension-two Turing-Hopf point are reviewed. Section IV shows that the predicted dynamics can indeed be observed in numerical simulations of the semiconductor model. A comparison with a chemical reaction-diffusion model is made in Sec. V before we conclude.

II. LINEAR STABILITY ANALYSIS

We study the following dimensionless reaction-diffusion system [30,31]:

 © 1997 The American Physical Society

$$\frac{\partial a(x,t)}{\partial t}=\frac{u-a}{(u-a)^2+1}-Ta+\frac{\partial^2 a}{\partial x^2}, \tag{1}$$

$$\frac{\partial u(x,t)}{\partial t}=\alpha[j_0-(u-a)]+D\frac{\partial^2 u}{\partial x^2}. \tag{2}$$

It describes charge transport in a layered semiconductor device with a bistable current-voltage characteristic with an internal degree of freedom $a(x,t)$, e.g., an interface charge density, whose dynamics is governed by the nonlinear transport equation (1). Equation (2) describes the dielectric relaxation of the normalized voltage $u(x,t)$ across the device. Here j_0 is the normalized external current; α, which is proportional to $1/(C+C_{\rm ext})$, where C and $C_{\rm ext}$ are the internal and a parallel external capacitances, respectively, defines the time scale; D is an effective diffusion constant; and T is an internal system parameter. The variable a acts as an activator, and u acts as an inhibitor in terms of nonlinear dynamics [33]. In terms of the semiconductor model the quantity $u-a$ corresponds to the current density which is the physical quantity of interest. Throughout the paper all variables are measured in dimensionless units.

Under current control, i.e., fixed control parameter j_0, the model has a unique homogeneous fixed point

$$a^*=\frac{j_0}{T(j_0^2+1)}, \quad u^*=j_0+a^*. \tag{3}$$

To perform a linear stability analysis, we linearize the dynamic system (1)-(2) around the spatially homogeneous fixed point (3) for small space- and time-dependent fluctuations $(\delta a,\delta u)\sim\exp(\lambda t+ikx)$, and obtain the characteristic equation

$$\lambda^2-\Theta\lambda+\Delta=0, \tag{4}$$

where

$$\Theta(k)=\gamma-T-\alpha-(D+1)k^2, \tag{5}$$

$$\Delta(k)=\alpha T+(\alpha-\gamma D+DT)k^2+Dk^4, \tag{6}$$

with

$$\gamma=\frac{j_0^2-1}{(j_0^2+1)^2}. \tag{7}$$

The physical control parameter of the system is the current density j_0. To simplify the formalism, we will use the parameter γ as the bifurcation parameter. The physical parameter j_0 can always easily be found once γ is fixed. Note, however, that the relation

$$j_0^2=(1\pm\sqrt{1-8\gamma})/(2\gamma)-1 \tag{8}$$

yields two positive values of j_0 in the range $0<\gamma<\frac{1}{8}$, since $\gamma(j_0)$ is nonmonotonic (see Fig. 1). As additional control parameters we will use the ratio α of the time scales of a and u (which can be varied by changing the external capacitor), the effective diffusion constant D (which is the squared ratio

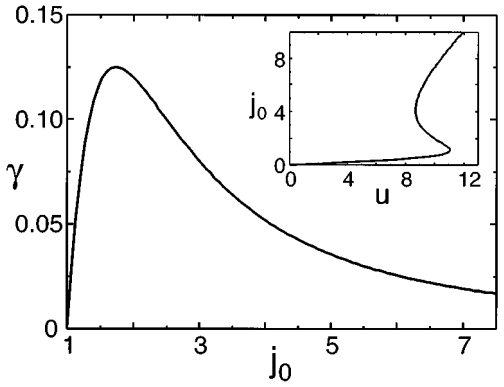

FIG. 1. Bifurcation parameter γ as a function of the physical control parameter j_0. The inset shows the normalized static current-voltage characteristic for $T=0.05$.

of the two intrinsic length scales of u and a), and the system size L. The parameter $T=0.05$ will be kept fixed throughout the following.

The roots of Eq. (4) yield the dispersion relation

$$\lambda_{1,2}(k)=\tfrac{1}{2}[\Theta\pm\sqrt{\Theta^2-4\Delta}]. \tag{9}$$

Modes with $\mathrm{Re}(\lambda)>0$ are unstable. We use Neumann boundary conditions $\partial a/\partial x=\partial u/\partial x=0$ for $x=0$ and L. The Neumann boundary conditions allow only cosine modes $\cos(kx)$, where $k=n\pi/L$ with integer n. For those unstable modes the real and imaginary parts of λ are plotted versus k for different values of α and j_0 in Figs. 2(a) and 2(b). It can be seen that instabilities occur in two ranges of k values around $k=0$ (Hopf modes) and around a finite value $k=k_c$ (Turing modes). The homogeneous steady state becomes unstable against the homogeneous mode $k=0$, and then evolves toward a spatially homogeneous limit cycle when the bifurcation parameter γ (or equivalently j_0) is increased above the Hopf threshold of instability,

$$\gamma^H=\alpha+T. \tag{10}$$

At the bifurcation point, the frequency of these temporal oscillations is given by $\omega_c=\mathrm{Im}(\lambda)=\sqrt{\Delta(k=0)}$, i.e.,

$$\omega_c=\sqrt{\alpha T}. \tag{11}$$

A Turing instability occurs above the Turing threshold

$$\gamma^T=\left[\sqrt{T}+\left(\frac{\alpha}{D}\right)^{1/2}\right]^2, \tag{12}$$

leading to the bifurcation of stationary spatially periodic patterns characterized by the intrinsic wave vector k_c with

$$k_c^2=\left(\frac{\alpha T}{D}\right)^{1/2}. \tag{13}$$

In Fig. 3, the curves at which the Hopf and Turing instabilities occur are plotted in the (α,j_0) control parameter space for fixed $T=0.05$ and $D=8$. Below the full line (Hopf bifurcation) the homogeneous steady state is unstable with respect to homogeneous temporal oscillations, and below the dashed

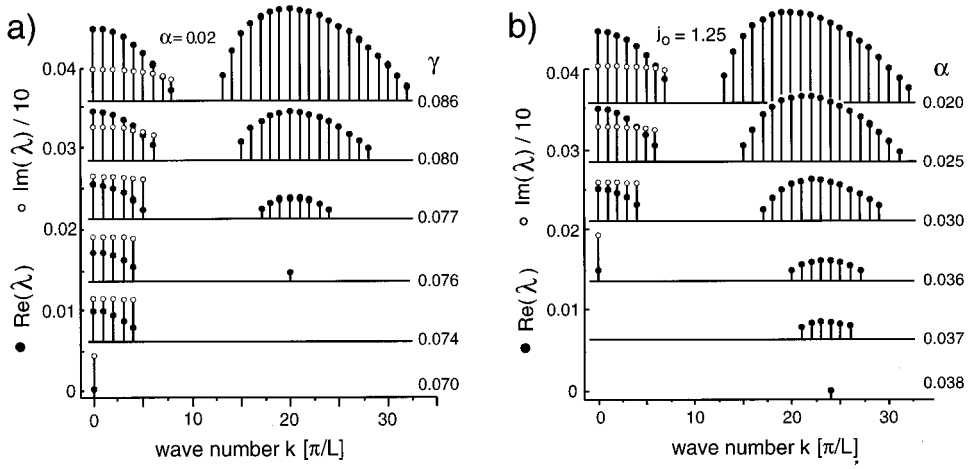

FIG. 2. Dispersion relation for different values of (a) γ (equivalently j_0) and (b) α. Re(λ) (full circles) and Im(λ) (open circles) are plotted vs the wave vector $k=n\pi/L$ in units of π/L only for unstable modes. In (a) $\alpha=0.02$ and in (b) $j_0=1.25$ are fixed. ($D=8$, $T=0.05$, and $L=600$.)

line (Turing instability) it is unstable with respect to stationary spatially periodic patterns. In the overlap of both instability regimes there is a competition between temporal and spatial symmetry-breaking instabilities. This can lead to an interaction of both types, producing particularly complex spatiotemporal patterns if the thresholds for both instabilities occur close to each other. This is the case in the vicinity of degenerate points (marked by C_1 and C_2), where the Hopf and the Turing bifurcations coincide: these are called *codimension-two Turing-Hopf points* (CTHP's), because two control variables are necessary to fix these bifurcation points in a generic system of equations. At the codimension-two Turing-Hopf points (C_1, C_2), we have $\gamma^T=\gamma^H$; in other words,

$$\alpha+T=\left[\sqrt{T}+\left(\frac{\alpha}{D}\right)^{1/2}\right]^2. \tag{14}$$

For a given α, this condition is satisfied for the critical value of D:

$$D_c=\left[\left(1+\frac{T}{\alpha}\right)^{1/2}-\left(\frac{T}{\alpha}\right)^{1/2}\right]^{-2}. \tag{15}$$

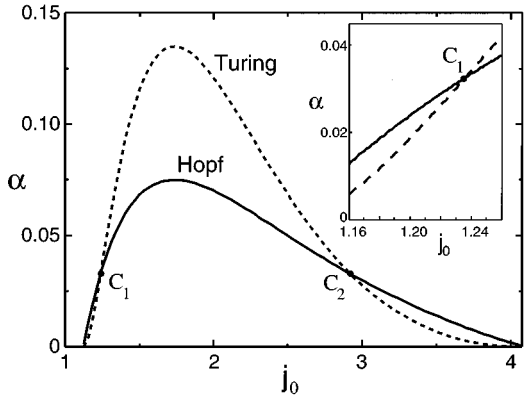

FIG. 3. Instability regimes in the (α,j_0) control parameter diagram for $T=0.05$ and $D=8$. The full and dashed lines denote the Hopf bifurcation and the Turing instability, respectively. The codimension-two Turing-Hopf points (CTHP) are marked by C_1 and C_2. The inset shows the vicinity of C_1 in an enlarged scale.

If $D<D_c$, it follows from Eqs. (10) and (12) that $\gamma^H<\gamma^T$, and, hence, with increasing γ (corresponding to increasing j_0 near C_1, or decreasing j_0 near C_2), the Hopf threshold is the first to be crossed and hence the Hopf instability will be the first to occur near criticality. If $D>D_c$, on the contrary, the first bifurcation will occur toward Turing patterns. For fixed D, codimension-two Turing-Hopf points occur at

$$\alpha_c=\frac{4DT}{(D-1)^2}, \tag{16}$$

which yields the two points (C_1 and C_2) at $\alpha_c\approx0.033$ marked in Fig. 3. If $\alpha<\alpha_c$, with increasing j_0, the Hopf bifurcation is the first to occur. For $\alpha>\alpha_c$, on the contrary, the Turing bifurcation appears first. This can be seen more clearly in the inset of Fig. 3, which shows the region near C_1 in an enlarged scale.

In summary, there is a one-parameter family of CTHP's if we consider the control parameters α, D, and j_0 as adjustable parameters. The projections of this curve onto the three coordinate planes in (α, D, j_0) control parameter space is shown in Fig. 4. We would like to see now which dynamics will be observed in the semiconductor model near a CTHP. Let us first review the dynamics predicted theoretically.

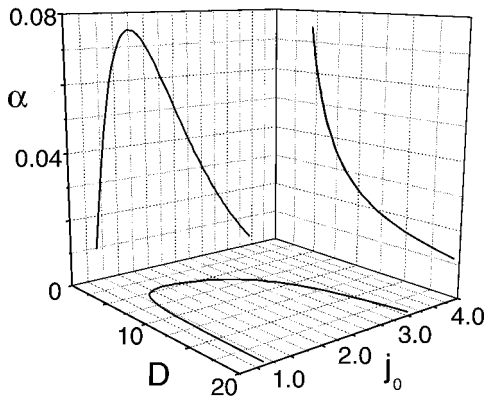

FIG. 4. Projections of the curve of CTHP's onto the three coordinate planes of the (α,D,j_0) control parameter space ($T=0.05$).

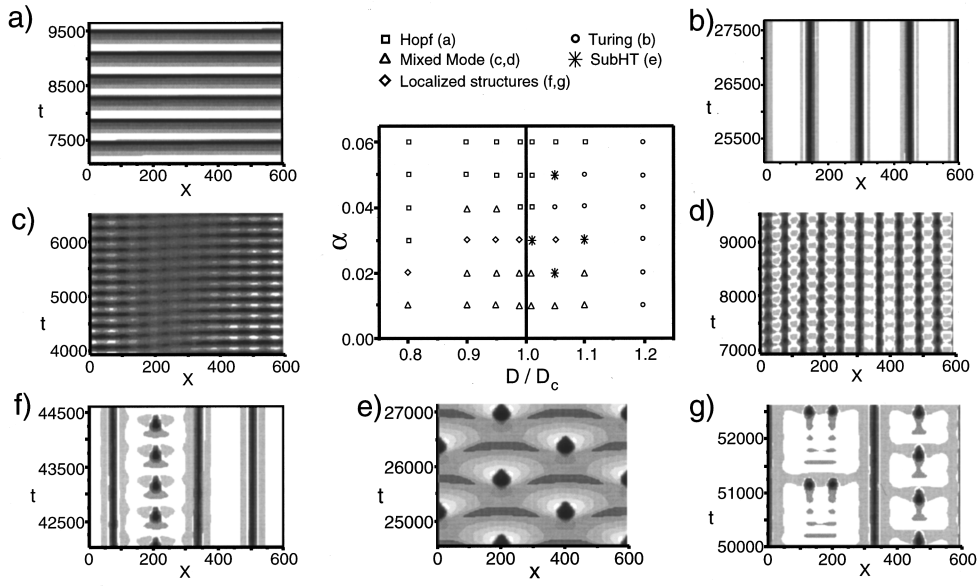

FIG. 5. Regimes of different asymptotic spatiotemporal behavior near the CTHP bifurcation given by the line $D/D_c=1$. The symbols in the $(\alpha,D/D_c)$ control parameter space denote various types of space-time patterns which are illustrated by typical space-time plots of $j(x,t)$ as insets: (a) Hopf oscillations (squares), (b) Turing patterns (dots), (c) and (d) Turing-Hopf mixed modes (triangles), (e) subharmonic Turing-Hopf mode consisting of spatiotemporal spiking (asterisks), and (f) and (g) localized Turing-Hopf structures (diamonds). (For parameters, see Table I.)

III. SPATIOTEMPORAL DYNAMICS NEAR THE CODIMENSION-TWO TURING-HOPF POINT

Near the CTHP, the linear stability analysis thus features degeneracy between a real root vanishing for a wave number k_c and a pair of complex conjugate roots with zero real part and frequency ω_c. Several analyses [6–10] in one-dimensional systems have already studied the bifurcation scenarios resulting from the interaction of the related modes, i.e., the spatial Turing mode characterized by the wave-number frequency couple $(k_c,0)$ and the temporal Hopf mode $(0,\omega_c)$. Let us briefly review these bifurcations schemes as they will be used to classify the spatiotemporal dynamics observed numerically in the semiconductor model.

In the vicinity of a CTHP, the bifurcation scenarios can be divided into two main groups. The first one gathers the dynamics resulting from the interaction between the Turing mode $(k_c,0)$ and the Hopf mode $(0,\omega_c)$. It has been shown [6,8,9], using amplitude equations formalism [35], that the competition between these two modes can lead to three different solutions which are the pure Turing structure, the pure Hopf oscillation, and a mixed mode (k_c,ω_c) consisting of a Turing pattern oscillating globally in time [36]. Depending on the specific parameters of the system [10], the relative stability of these three solutions leads to two bifurcation scenarios: either the mixed mode is always unstable while the Turing and Hopf states are bistable in a given domain of the control parameter, or the mixed mode is stable for values of parameters for which the Turing and Hopf modes are both unstable. The coupling between the Turing and the Hopf modes thus leads to either Turing-Hopf bistability or a mixed mode with one wave number and one frequency.

The second main group of dynamics near the CTHP results from subharmonic instabilities [37–40] of the pure Turing or Hopf modes. Let us first consider the Turing mode with wave number k_c. Close to the CTHP, its subharmonic mode with wave number $k_c/2$ may have a complex linear eigenvalue with a small growth rate and a frequency $\omega[k_c/2]$. Near the CTHP, a resonant interaction between the two modes $(k_c,0)$ and $(k_c/2,\omega[k_c/2])$ can give rise to a stable mixed state called a subharmonic Turing mixed mode [40], or also in short, a sub-T mode. This mixed solution corresponds to a spatial structure with two wave numbers (k_c and $k_c/2$) oscillating in time with one frequency ($\omega[k_c/2]$). An analogous subharmonic instability can also occur if the system is originally in a pure Hopf state with frequency ω_c. If the control parameter is increased, a resonant interaction between this Hopf mode and the subharmonic mode $(k[\omega_c/2],\omega_c/2)$ can occur. The stable solution resulting from this interaction is then a subharmonic Hopf mixed mode [10], or in short a sub-H mode characterized by two frequencies (ω_c and $\omega_c/2$) and one wave number ($k[\omega_c/2]$). In the particular case where $k[\omega_c/2]$ is of the order of the subharmonic wave number of the Turing mode, i.e., $k\approx k_c/2$, another mixed state with two wave numbers ($k[\omega_c/2]$ and $2k\approx k_c$) and two frequencies (ω_c and $\omega_c/2$) can be observed. This mixed solution is coined a subharmonic Turing-Hopf mode [10] or also a sub-HT mode as it results from the resonance near the CTHP of a sub-H mode and a Turing mode.

In short, the spatiotemporal dynamics near a CTHP feature either bistability between steady structures and temporal oscillations or various mixed states ranging from the simple Turing-Hopf mixed mode to different types of subharmonic modes. Let us note that, in large systems, each of these solutions can undergo phase instabilities for given values of the parameters, giving rise to spatiotemporal chaos. The Benjamin-Feir and Eckhaus instabilities are the well-known phase instabilities of the pure Hopf and Turing modes, respectively [35]. Conditions have also been given for which the Turing-Hopf mixed mode [36] and the sub-T mode [40] become chaotic due to a phase instability.

IV. SPATIOTEMPORAL DYNAMICS IN A SEMICONDUCTOR MODEL

Let us now verify if the different predicted types of dynamics can be recovered in models (1) and (2). These equations are solved using finite differences and a forward Euler algorithm. A systematic overview of the different dynamical behavior can be gained by investigating the various regimes

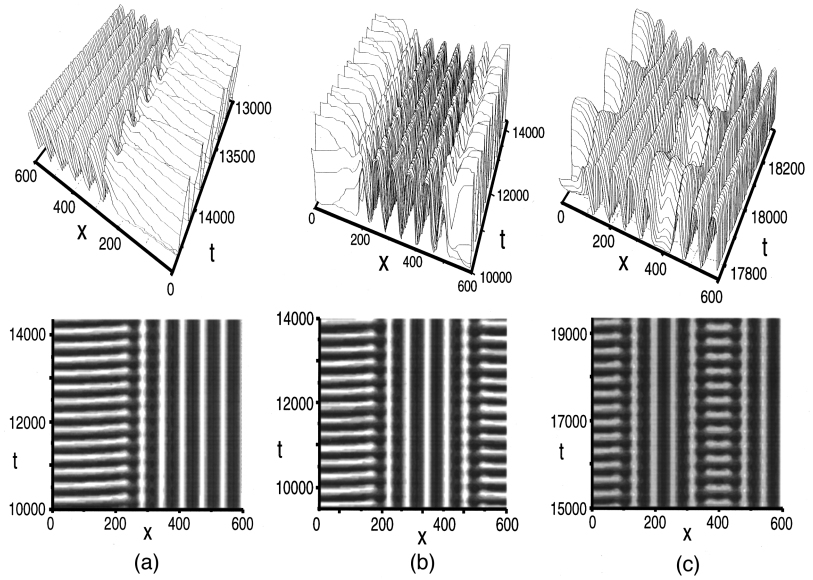

FIG. 6. Localized structures near the CTHP C_2 for $T=0.05$, $\alpha=0.02$, $D=8$ (corrresponding to $D/D_c=0.67$), $j_0=3.1$, and different initial conditions: (a) Turing-Hopf front. (b) Turing domain embedded between two Hopf states. (c) Localized Turing-Hopf structures. The current density $j(x,t)$ is shown as a density plot and as a three-dimensional representation.

in a diagram of α versus D/D_c (Fig. 5). In physical units, this diagram corresponds to the ratio of time scales τ_a/τ_u versus the ratio of the squared length scales l_a^2/l_u^2 of the two variables a and u, respectively. By normalizing D by its critical value $D_c(\alpha)$ for each α, we transform all codimension-two Turing-Hopf points onto the straight line $D/D_c=1$. As discussed before, for $D/D_c>1$ the Turing instability occurs first with increasing j_0, while for $D/D_c<1$ the Hopf bifurcation occurs first. Therefore, on the right-hand side of the diagram, the Turing modes are expected to be dominant near criticality, while on the left-hand side this applies to the Hopf modes. For various points in the parameter space of Fig. 5, model (1)-(2) has been integrated starting from random initial conditions. Typical space-time plots which are observed at different j_0 values near the Turing-Hopf point C_1 (Fig. 3) are shown as insets. It should, however, be noted that depending upon the initial conditions, the obtained asymptotic behavior can be quite different. If j_0, and thus γ, is chosen above the first instability threshold γ^H or γ^T, and D/D_c is sufficiently far from the Turing-Hopf point ($D/D_c=1$), then the only patterns found are indeed pure Hopf oscillations [Fig. 5(a)] (for $D/D_c<1$) or Turing structures [Fig. 5(b)] (for $D/D_c>1$). If D/D_c approaches unity, the spatial and temporal modes may interact leading to the various types of dynamics predicted theoretically. The Turing-Hopf mixed mode with one wave number and one frequency is recovered near the codimension-two line [see Fig. 5(d)]. In large systems, the temporal oscillations of the mixed mode might not be exactly in phase, as shown in Fig. 5(c). Some of the subharmonic mixed states have also been obtained in our semiconductor model. Figure 5(e) presents an example of the sub-HT mode characterized by two wave numbers and two frequencies. The original frequency ω_c and wave vector k_c are still visible in the alternating spatial and temporal shift of the pattern by one period in space and in time. This is the periodic spatiotemporal spiking mode which was found and discussed previously [31]. We have now gained a more profound understanding of its nature. It naturally appears due to the interaction of spatial and temporal symmetry breaking instabilities close to CTHP's.

Other types of dynamics occur at other points in the $(\alpha,D/D_c)$ diagram [Figs. 5(f) and 5(g)] or when the bifurcation parameter j_0 is further increased. In particular, the bistability between Turing and Hopf modes predicted theoretically is obtained for several values of parameters. In the bistability regime, localized Turing-Hopf structures such as droplets of one state embedded into the other or fronts between a Turing pattern and an oscillating region are commonly observed [3,4,10]. In Fig. 5(f), a spiking ''droplet'' is embedded in a Turing structure, and in Fig. 5(g) a Turing structure is embedded in a complex oscillating state. For much larger j_0 in the vicinity of the second CTHP C_2, spatial coexistence of a Hopf oscillation and a Turing structure are obtained (Fig. 6). Depending upon the initial conditions, different localized structures occur: a Turing-Hopf front with a fixed boundary between the two phases [Fig. 6(a)], Turing domains embedded between two Hopf states [Fig. 6(b)], or alternating sequences of localized Hopf and Turing domains [Fig. 6(c)] are found. Similar behavior has been found in other two-component reaction-diffusion systems [3,4,10]. Such localized, coexisting structures indicate that in this range of parameters there is bistability between Turing and Hopf modes, in contrast to the mode mixing which is effective at lower values, near the CTHP C_1. It may be conjectured that this different behaviour is related to the asymmetry of the reaction term in Eq. (1), as discussed in Ref. [30]. There it was noted, for a slightly different model with only one diffusion length and a global coupling term, that the condition for spatial coexistence of two bistable homogeneous phases is satisfied at a value of u_{co} on the left-hand side of the bistability range of the $j_0(u)$ characteristic, while spiking, in contrast, was only found on the very right-hand edge of the characteristic. In fact, C_1, where spiking and mixed modes occur, is located at a j_0 value in the right-hand corner of the characteristic (cf. the inset of Fig. 1), while C_2, where localized bistable structures are found, lies in the left-hand corner close to the coexistence value u_{co} of the model with one length scale. The asymmetry of model (1)-(2) can be seen by plotting the period of homogeneous temporal oscillations for two different values of α (see Fig. 7). The period of the oscillations varies strongly above the Hopf

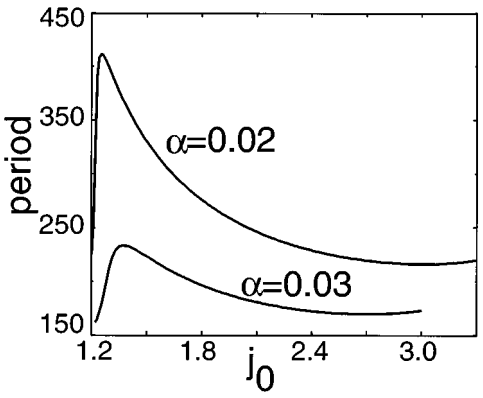

FIG. 7. Period of the temporal oscillations as a function of j_0 for two values of α. These periods are obtained by integrating models (1) and (2) without diffusion such that the Hopf instability is the only one possible.

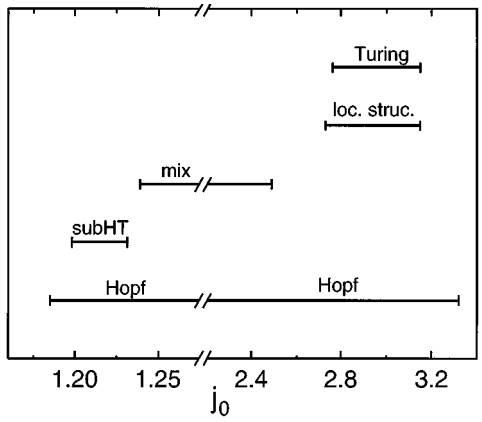

FIG. 8. Stability regimes of various patterns as a function of j_0 for $T=0.05$, $\alpha=0.02$, and $D=8$. ''mix'' stands for the Turing-Hopf mixed mode with one wave number and one frequency. Note that localized structures (''loc. struc.'') are observed for values of parameters where the Turing and Hopf modes are bistable.

threshold C_1 and this variation increases when α is decreased.

A detailed analysis of a bifurcation scenario as a function of j_0 is made in Fig. 8 for a given set of parameters α and D and summarizes the above explanations. The stability range of the different spatiotemporal patterns is schematically indicated. The Hopf oscillation persists throughout the range of j_0 values between the two Hopf bifurcations (cf. Fig. 3). In the immediate vicinity of the thresholds C_1 and C_2, the period of the oscillations is that given by the linear stability analysis (compare the values for ω_c and k_c found by linear stability analysis at the Hopf or Turing instability, respectively, and the corresponding temporal and spatial periods $\tau_c=2\pi/\omega_c$ and $\Lambda_c=2\pi/k_c$ listed in Table I), while this period increases strongly near $j_0=1.25$ (see Fig. 7). The subharmonic Hopf-Turing (sub-HT) spiking mode exists only for low values of j_0 near C_1, and localized structures and the pure Turing mode are found at higher values near C_2. Note that as the localized structures are due to a Turing-Hopf bistability, they exist in the range of j_0 for which the pure Turing and Hopf modes are both observed. The Turing-Hopf mixed mode with one wave number and one frequency appears in a wide intermediate range between these two ends. We have noticed that, near C_2, the wavelength of the Turing mode is that given by the linear stability analysis. If j_0 is then decreased, this wavelength increases strongly, and can become almost twice the one predicted by the linear stability analysis in the vicinity of C_1. This explains why all spatiotemporal dynamics slightly above C_2 exhibit periods and wavelengths much greater than those predicted by the linear stability analysis. By choosing different initial conditions, multistability between some of these patterns can be realized as indicated. In general, all mixed modes disappear in favor of either a Hopf or a Turing mode if the parameters α and D are sufficiently far from the CTHP's.

Further, it should be noted that the asymptotic patterns are preceded in general by transient spatiotemporal chaos when random initial conditions are used, as analyzed in detail by Wacker, Bose, and Schöll [31], and that the transient times are often so long that the asymptotic state is not observed. However, as pointed out before, all the different dynamics observed can exhibit phase instabilities under certain conditions. A nonlinear stability analysis giving the conditions for the occurrence of these phase instabilities in terms of the parameters of our model should be performed in order to see whether these spatiotemporal chaotic regimes are only long transients or if they describe intrinsic dynamics of the system.

TABLE I. Parameters used in the simulations ($L=600$ and $T=0.05$ everywhere). ω_c and τ_c are the critical Hopf frequency and period, respectively. k_c is the critical Turing wave number, and Λ_c the corresponding wavelength.

	α	D	D/D_c	j_0	ω_c	τ_c	k_c	Λ_c
Fig. 5(a)	0.0250	8.0000	0.81	1.2500	0.0354	178	0.1118	56.2
(b)	0.0200	14.2993	1.20	1.1912	0.0316	199	0.0914	68.7
(c)	0.0300	8.6352	1.01	1.2247	0.0387	162	0.1148	54.7
(d)	0.0381	8.0000	1.12	1.2500	0.0436	144	0.1242	50.6
(e)	0.0100	10.7245	0.49	1.1622	0.0224	281	0.0826	76.0
(f)	0.0200	12.0353	1.01	1.1851	0.0316	199	0.0955	65.8
(g)	0.0200	12.5120	1.05	1.1838	0.0316	199	0.0946	66.5
Fig. 6	0.0200	8.0000	0.67	3.1000	0.0316	199	0.1057	59.4
Fig. 8	0.0200	8.0000	0.67					

TABLE II. Comparison between the semiconductor activator-inhibitor system and the Brusselator chemical reaction-diffusion system.

	Semiconductor	Brusselator
Bifurcation parameter	γ	B
Ratio of diffusion coefficients	$1/D$	$D_x/D_y=\sigma$
Hopf threshold	$\gamma^H=T+\alpha$	$B^H=1+A^2$
Hopf frequency ω_c	$\sqrt{\alpha T}$	A
Turing threshold	$\gamma^T=\left(\sqrt{T}+\sqrt{\frac{\alpha}{D}}\right)^2$	$B^T=(1+A\sqrt{\sigma})^2$
Turing wave number k_c^2	$\sqrt{\frac{\alpha T}{D}}$	$\frac{A}{\sqrt{D_xD_y}}$
Codimension-two Turing-Hopf point	$D_c=[(\sqrt{T+\alpha}-\sqrt{T})/\sqrt{\alpha}]^{-2}$	$\sigma_c=[(\sqrt{1+A^2}-1)/A^2]^2$

V. COMPARISON WITH THE BRUSSELATOR MODEL

The behavior found in the reaction-diffusion model (1)-(2) is quite similar to that obtained for the Brusselator model of chemical active media [41]

$$\partial_t X=A-(B+1)X+X^2Y+D_x\nabla^2X,$$

$$\partial_t Y=BX-X^2Y+D_y\nabla^2Y, \tag{17}$$

where X and Y are the concentrations of two intermediate chemical species, A and B are the concentrations of the reactants that are kept constant, and D_x and D_y are diffusion constants. B is the control parameter. A straightforward comparison between the Brusselator model (17) and the semiconductor model (1)-(2) can be achieved if we consider the following equivalences:

$$\sqrt{\alpha}=A, \tag{18}$$

$$D=1/\sigma. \tag{19}$$

The corresponding thresholds of instabilities and other characteristics of the two systems are given in Table II. The Brusselator also generically exhibits both Turing and Hopf instabilities, and hence allows for a CTHP. An important difference between the two models is that, in the Brusselator, once $(A,\sigma/\sigma_c)$ is fixed, one has only one CTHP while in the semiconductor model two CTHP's exist for given values of $(\alpha,D/D_c)$.

Recently, the spatiotemporal dynamics occurring in the Brusselator near the CTHP has also been studied [10]. It is interesting to note that, there, bistability (and related localized structures) and simple as well as the subharmonic mixed modes have also been observed. In that case the spatiotemporal self-organization is that of chemical concentrations rather than of the current density in our model. In the Brusselator, the spatiotemporal dynamics near the CTHP has been classified in the A versus σ/σ_c control parameter space where $\sigma=D_x/D_y$, i.e., in the ''time scale'' versus ''space scale'' plane. Strikingly, this classification presents strong similarities with the one shown for our semiconductor model in Fig. 5. As an example, the successive bifurcations displayed in Fig. 8 are analogous to some observed in the Brusselator model (see Fig. 12 of Ref. [10]). This similarity of behavior might suggest that independently of the characteristics of the reaction-diffusion system at hand, the spatiotemporal dynamics in the vicinity of a CTHP might be classified generically in a ''time scale'' versus ''space scale'' plane.

VI. CONCLUSION

Starting from a generic semiconductor model which describes charge transport through a semiconductor device, we showed that the interaction of the two instabilities occurring in this model (Hopf and Turing) yields complex spatiotemporal patterns. As a result we can find a variety of interesting patterns which are the result of either bistability between Turing and Hopf patterns or a mixing of these modes. Some of these structures, like the subharmonic Turing-Hopf spiking mixed states, have already been observed experimentally in p-i-n diodes [21], but for the localized patterns and the Turing-Hopf mixed mode there is, to the best of our knowledge, no experimental evidence yet. It is difficult to detect such structures in semiconductor experiments, because of the small size of the system and the high spatial and temporal resolution required. However, because of the direct modulation of the total current by those spatiotemporal patterns, the rich variety of possible spatiotemporal modes should be of considerable interest with respect to potential applications, e.g., like tunable semiconductor oscillators.

The stability of the different spatiotemporal dynamics observed near the codimension-two Turing-Hopf point in the semiconductor model can be explained in the framework of the amplitude equations formalism [10]. These types of dynamics are hence generic of the CTHP, and are qualitatively similar to those observed near a CTHP in a chemical reaction-diffusion model; however some structures which occur in the chemical model, e.g., the subharmonic Turing mixed mode, have not yet been found in our semiconductor model. Another difference is the large variation of the spatial wavelength and of the temporal period near the first bifurcation point C_1 in the semiconductor model, an effect which is not observed in the chemical model.

We propose that a time-scale versus length-scale diagram might be an appropriate way for organizing the comparison of other models featuring codimension-two Turing-Hopf points because it separates out the different scales which reflect the spatial character of the Turing mode and the tempo

ral character of the Hopf mode. In this sense, this type of diagram might be useful in looking for the predicted spatiotemporal dynamics characteristic of the coupling between spatial and temporal modes in any model featuring an interaction between a steady instability (not necessarily the Turing one) and a Hopf instability.

ACKNOWLEDGMENT

Stimulating discussions with H. Engel, A. Wacker, D. Lima, P. Borckmans, and G. Dewel and partial support by Deutsche Forschungsgemeinschaft, are acknowledged. A. D. acknowledges support by the FNRS (Belgium).

[1] P. Kolodner, Phys. Rev. E **48**, R665 (1993).
[2] D.P. Vallette, W.S. Edwards, and J.P. Gollub, Phys. Rev. E **49**, R4783 (1994).
[3] G. Heidemann, M. Bode, and H.-G. Purwins, Phys. Lett. A **177**, 225 (1993).
[4] J.-J. Perraud, A. De Wit, E. Dulos, P. De Kepper, G. Dewel, and P. Borckmans, Phys. Rev. Lett. **71**, 1272 (1993).
[5] P. De Kepper, J.-J. Perraud, B. Rudovics, and E. Dulos, Int. J. Bifurc. Chaos Appl. Sci. Eng. **4**, 1215 (1994).
[6] J.P. Keener, Stud. Appl. Math. **55**, 187 (1976).
[7] G. Nicolis, T. Erneux, and M. Herschkowitz-Kaufman, Adv. Chem. Phys. **38**, 263 (1978).
[8] H. Kidachi, Prog. Theor. Phys. **63**, 1152 (1980).
[9] J. Guckenheimer and P. Holmes, *Nonlinear Oscillations, Dynamical Systems, and Bifurcations of Vector Fields* (Springer-Verlag, New York, 1983).
[10] A. De Wit, D. Lima, G. Dewel, and P. Borckmans, Phys. Rev. E **54**, 261 (1996).
[11] A. Turing, Philos. Trans. R. Soc. London, Ser. B **237**, 37 (1952).
[12] P. Borckmans, G. Dewel, A. De Wit, and D. Walgraef, in *Chemical Waves and Patterns*, edited by R. Kapral and K. Showalter (Kluwer, Dordrecht, 1995), p. 323, and references therein.
[13] E. Schöll, *Nonequilibrium Phase Transitions in Semiconductors* (Springer, Berlin, 1987).
[14] M. P. Shaw, V. V. Mitin, E. Schöll, and H. L. Grubin, *The Physics of Instabilities in Solid State Electron Devices* (Plenum, New York, 1992).
[15] B. S. Kerner and V. V. Osipov, *Autosolitons* (Kluwer, Dordrecht, 1994).
[16] *Nonlinear Dynamics and Pattern Formation in Semiconductors and Devices*, edited by F.J. Niedernostheide (Springer, Berlin, 1995).
[17] A. Wacker and E. Schöll, J. Appl. Phys. **78**, 7352 (1995).
[18] A.V. Gorbatyuk and P.B. Rodin, J. Commun. Technol. Electron. **40**, 49 (1995).
[19] F.-J. Niedernostheide, M. Arps, R. Dohmen, H. Willebrand, and H.-G. Purwins, Phys. Status Solidi B 172, 249 (1992).
[20] F.-J. Niedernostheide, H. J. Schulze, S. Bose, A. Wacker, and E. Schöll, Phys. Rev. E **54**, 1253 (1996).
[21] R. Symanczyk, S. Gaelings, and D. Jäger, Phys. Lett. A **160**, 397 (1991).
[22] U. Rau, W. Clauss, A. Kittel, M. Lehr, M. Bayerbach, J. Parisi, J. Peinke, and R. P. Huebener, Phys. Rev. B **43**, 2255 (1991).
[23] J. Spangler, U. Margull, and W. Prettl, Phys. Rev. B **45**, 12 137 (1992).
[24] B. Kerner and V. Osipov, Zh. Eksp. Teor. Fiz. **83**, 2201 (1982) [Sov. Phys. JETP **56**, 1275 (1982)].
[25] B. Kerner and V. Osipov, Usp. Fiz. Nauk **157**, 201 (1989) [Sov. Phys. Usp. **32**, 101 (1989)].
[26] H. Willebrand, T. Hünteler, F. J. Niedernostheide, R. Dohmen, and H. G. Purwins, Phys. Rev. A **45**, 8766 (1992).
[27] F.-J. Niedernostheide, B. S. Kerner, and H.-G. Purwins, Phys. Rev. B **46**, 7559 (1992).
[28] F.-J. Niedernostheide, M. Ardes, M. Or-Guil, and H.-G. Purwins, Phys. Rev. B **49**, 7370 (1994).
[29] M. Bode and H. Purwins, Physica D **86**, 53 (1995).
[30] A. Wacker and E. Schöll, Z. Phys. B **93**, 431 (1994).
[31] A. Wacker, S. Bose, and E. Schöll, Europhys. Lett. **31**, 257 (1995).
[32] A. Wacker and E. Schöll, Semicond. Sci. Technol. **9**, 592 (1994).
[33] A.S. Mikhailov, *Foundations of Synergetics 1*, 2nd ed. (Springer, Berlin, 1994).
[34] *Self-Organization in Activator-Inhibitor-Systems: Semiconductors, Gas Discharge, and Chemical Active Media*, edited by H. Engel, F.J. Niedernostheide, H.G. Purwins, and E. Schöll (Wissenschaft und Technik Verlag, Berlin, 1996).
[35] M.C. Cross and P.C. Hohenberg, Rev. Mod. Phys. **65**, 851 (1993).
[36] A. De Wit, G. Dewel, and P. Borckmans, Phys. Rev. E **48**, R4191 (1993).
[37] A. Hill and I. Stewart, Dyn. Stab. Syst. **6**, 149 (1991).
[38] M. Cheng and H.-C. Chang, Phys. Fluids A **4**, 505 (1992).
[39] K. Fujimura and Y. Renardy, Physica D **85**, 25 (1995).
[40] D. Lima, A. De Wit, G. Dewel, and P. Borckmans, Phys. Rev. E **53**, R1305 (1996).
[41] G. Nicolis and I. Prigogine, *Self-Organization in Nonequilibrium Systems* (Wiley, New York, 1977).